Gravity current down a steeply inclined slope in a rotating fluid

G. I. Shapiro, A. G. Zatsepin

Ann. Geophysicae 15, 366–374 (1997) © EGS – Springer-Verlag 1997

Annales Geophysicae

Gravity current down a steeply inclined slope in a rotating fluid

G. I. Shapiro, A. G. Zatsepin

P.P. Shirshov Institute of Oceanology, 23 Krasikova str. 117218 Moscow, Russia

Received: 3 November 1995/Revised: 16 September 1996/Accepted: 17 September 1996

Abstract. The sinking of dense water down a steep continental slope is studied using laboratory experiments, theoretical analysis and numerical simulation. The experiments were made in a rotating tank containing a solid cone mounted on the tank floor and originally filled with water of constant density. A bottom gravity current was produced by injecting more dense coloured water at the top of the cone. The dense water plume propagated from the source down the inclined cone wall and formed a bottom front separating the dense and light fluids. The location of the bottom front was measured as a function of time for various experimental parameters. In the majority of runs a stable axisymmetric flow was observed. In certain experiments, the bottom layer became unstable and was broken into a system of frontal waves which propagated down the slope. The fluid dynamics theory was developed for a strongly non-linear gravity current forming a near-bottom density front. The theory takes into account both bottom and interfacial friction as well as deviation of pressure from the hydrostatic formula in the case of noticeable vertical velocities. Analytical and numerical solutions were found for the initial ($t < 1/f$), intermediate ($t \approx 1/f$), and main ($t \gg 1/f$) stages, where f is the Coriolis parameter. The model results show that during the initial stage non-linear inertial oscillations are developed. During the main stage, the gravity current is concentrated in the bottom layer which has a thickness of the order of the Ekman scale. The numerical solutions are close to the same analytical one. Stability analysis shows that the instability threshold depends mainly on the Froude number and does not depend on the Ekman number. The results of laboratory experiments confirm the similarity properties of the bottom front propagation and agree well with the theoretical predictions.

Introduction

The sinking of dense water over the continental slope is a significant contributor to water exchange between the shelf-slope zone and the open ocean. Dense water accumulates on shelves, migrates to the shelf edge, and flows across the continental slope forming a gravity current. This process is thought to be important in the formation of oceanic bottom and deep waters, and particularly of Antarctic bottom water (Whitehead, 1987). Other examples are bottom gravity currents in the South Australian Gulfs (Bowers and Lennon, 1987), the Denmark Straits overflow (Dickson *et al.*, 1990), the Mediterranean outflow into the Atlantic (Price *et al.*, 1993) and into the Black Sea (Latif *et al.*, 1991). Despite recent progress, bottom gravity currents over the continental slope have not been well investigated experimentally or theoretically. This is because, firstly, they often occur sporadically and in barely accessible regions, and secondly, the theoretical description of currents over a steep slope must be extended beyond geostrophic or quasi-geostrophic models to include friction and the vertical component of the Coriolis force.

In recent years, gravity currents on horizontal and inclined bottoms have been a subject of theoretical and laboratory studies (Zatsepin *et al.*, 1982; Shapiro, 1982; Kostianoy and Shapiro, 1985; Mory *et al.*, 1987; Simpson, 1987; Whitehead *et al.*, 1990; Speer *et al.*, 1993; Nagata *et al.*, 1993[1]; Zhmur *et al.,* 1994). The research has been restricted mainly to the case of a horizontal or slightly sloping bottom or a non-rotating fluid. In the theoretical studies, bottom friction has usually been considered in the "boundary layer" approximation (Whitehead, 1990; Speer *et al.*, 1993)

[1]This reference was brought to our attention by Dr. P. Baines after the manuscript had been submitted. In general, both the experiments and the theories are significantly different. However, one of our figures (Fig. 5) looks similar to Fig. 12 of Nagata et al. (1993)

Correspondence to: G. I. Shapiro

which is valid only if the thickness of the dense layer exceeds the vertical Ekman scale sufficiently. However, the laboratory experiments by Mory *et al.* (1987) indicated that the downslope plume was concentrated in a layer of the order of the Ekman scale. An intermediate situation has been observed in some natural environments (Latif *et al.*, 1991; Dickson *et al.*, 1990).

The purpose of this study is to achieve a better understanding of the mesoscale dynamics of gravity currents over a steeply inclined bottom in a rotating fluid for a wide range of Ekman numbers. The flow is studied by means of laboratory experiments, a theoretical analysis and numerical simulations. In this work we consider an axisymmetric two-layer problem: the dense fluid spreads below the light fluid over a conic surface from a source located on top of a cone and having a constant volume flux rate. The theoretical analysis is not restricted by the "boundary layer" approximation.

Experiment

Experimental set-up

The experiments were conducted on a rotating platform with a diameter of 1m. A rectangular perspex water tank of volume 50*50*46 cm^3 was set up in the centre of the platform, in the centre of which a circular plastic cone was mounted. The inclination angle of the cone wall was $\theta = 39^\circ$ (Fig. 1). The foot of the cone was fixed to the bottom of the tank and concentric circular labels were drawn on the cone surface at 2 cm intervals.

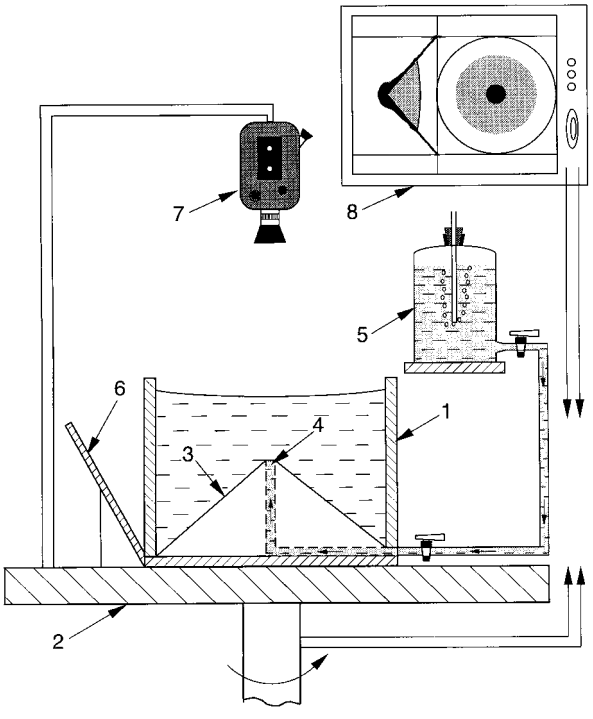

Fig. 1. Schematic diagram of the experimental set-up: 1, water tank; 2, rotating platform; 3, cone; 4, source of dense water, 5, Mariott bottle; 6, side view mirror; 7, video camera; 8 TV monitor

The platform had four fixed rates of rotation. The constancy of the rotation rate was checked with a strobe light. The period of rotation was measured by an electronic timer mounted on the platform. The tank was filled with a homogeneous aqueous solution of NaCl. The top and side views of the spreading process were documented by both video and photo cameras positioned on the platform above the tank. The side view was obtained using an inclined side mirror similar to the technique described by Mory *et al.* (1987).

At the beginning of each experiment the homogeneous fluid in the tank was spun up until it had reached the state of solid body rotation with angular velocity $\Omega = f/2$, where f is the Coriolis parameter. Salty water with a density higher than that of the ambient fluid was then injected at the top of the cone through an aperture with a diameter of 1 cm. The influx was kept constant during each experimental run by use of a Mariotte bottle. The injected fluid was coloured with thymol blue indicator to distinguish it from the ambient fluid. The location of the bottom front between dense and ambient fluids was observed on a TV monitor and recorded by the video camera continuously during each run.

The distance, L_f, between the front and the cone top was measured as a function of time, t, with $t = 0$ corresponding to the beginning of the injection. Readings were taken after each run from the TV monitor while the video tape was played back. The time marks were taken every time the front crossed the circular labels drawn on the inclined bottom between 7 cm and 29 cm labels. In order to improve the accuracy and exclude the error introduced by a slight deviation of the front from an exact axisymmetric shape, measurements were made independently along four different downslope directions. The four time marks corresponding to the same bottom label were then averaged. The root mean square deviation calculated for each group of four marks did not exceed 7%.

The value of the volume flux, Q, of the injected fluid was determined at the end of every experiment by dividing the total water consumption from the Mariotte bottle by the corresponding time interval. The salinity of both ambient and injected fluid was calculated using the weight method and measured with a laboratory salinometer. The weight of pure NaCl (ranging from 1 to 500 g) was measured with electronic scales with an accuracy of 10 mg. The density was then calculated from salinity. We determined the reduced gravity acceleration, g', by the formula $g' = g^*\Delta\rho/\rho$, where g^* is the acceleration due to gravity, $\Delta\rho$ is the density difference between the injected and the ambient water and ρ is the density of the ambient fluid. The relative error in determining Q and g' did not exceed 5%. The Coriolis parameter, f, was determined with an accuracy better than 0.5%. The viscosity of the water solution, ν was taken as 10^{-2} cm^2/s.

Experimental results

A set of 40 experimental runs was carried out for the following values of governing parameters: the source discharge $Q = 0.3 - 16.2$ cm^3/s, $f = 1.0 - 4.1$ rad/s, $g' = 0.3 - 12.5$ cm/s^2. The duration of each run was in the range 15 to 600 s.

The dense water, spreading from the source near the bottom, formed a nearly axisymmetric plume. Water in the plume rotated anticyclonically i.e. opposite to the rotation of the platform. The front of the gravity current gradually propagated downwards over the slope (Fig. 2A). The current appeared to be divided into two zones: a central, non-viscous, and a peripheral, viscous region (Zatsepin, 1986). In the central zone (with a diameter of no more than 10–15 cm) the thickness of the bottom layer was 1–3 cm which was much larger than the Ekman scale (which was about 0.1 cm) but was much less than the total height of water column above the cone (12–14 cm). Although the azimuthal velocity was not measured directly, the basic structure of the azimuthal flow was estimated by the visual analysis of the displacement of small dye inhomogenities of the dense fluid layer. The azimuthal velocity grew with the distance from the centre. In the peripheral zone the thickness of the gravity current was of the order of the Ekman scale. In this zone the anticyclonic circulation decreased with the distance. In some experiments small paper pellets were put on the surface of the top layer. These indicated no appreciable motion, except in cases where the thickness of the dense water plume in the central zone exceeded approximately 1/4 of the upper fluid depth. This condition was realised only during a few runs with small g' and large Q values. In the majority of experiments the upper fluid was at rest even in the central zone.

The functional dependence of L_f on t, Q, g', f was found using regression analysis of data over the whole set of experiments to be well approximated by the formula

$$L_f = AQ^m(g')'f^k t^n, \tag{1}$$

where : $A = 0.85 \pm 0.10, m = 0.24 \pm 0.02, l = 0.34 \pm 0.04$, $k = 0.26 \pm 0.03$, $n = 0.65 \pm 0.02$, with correlation coefficient $r = 0.95 \pm 0.01$. Deviation from Eq. (1) appeared at $Q > 15$ cm$^3/s$, $g' < 2$ cm$/s^2$ due to turbulent entrainment near the source and also at $Q < 0.3$ cm$^3/s$- probably due to the influence of the molecular diffusitivity on very thin and slow gravity currents.

The following parameters were estimated from the directly measured data: the downslope velocity of the front $u_f = dL_f/dt$, the effective thickness of the bottom layer $H^* = Q/(2\pi L_f u_f)$, the effective downslope Froude number $Fr^* = u_f/(g'H^*)^{1/2}$, the effective Reynolds number $Re^* = (u_f H^*)/\nu$, the effective Ekman number $E^* = (H_E/H^*)^2$, where $H_E = [\nu/(f\cos\theta)]^{1/2}$ is the Ekman scale. In the experiments, the Ekman scale was $H_E = 0.06 - 0.13$ cm whereas nondimensional parameters were in the range $Re^* = 0.21 - 26$, $Fr^* = 0.13 - 1.1$.

In certain experimental runs at slow rotation of the platform and large density differences between layers, the bottom layer was broken into a system of soliton-type frontal waves which propagated downwards (Fig. 2B.). At the transition between stable and oscillatory modes, a two-dimensional wave pattern was observed, the distance between crests being 2–4 cm. In

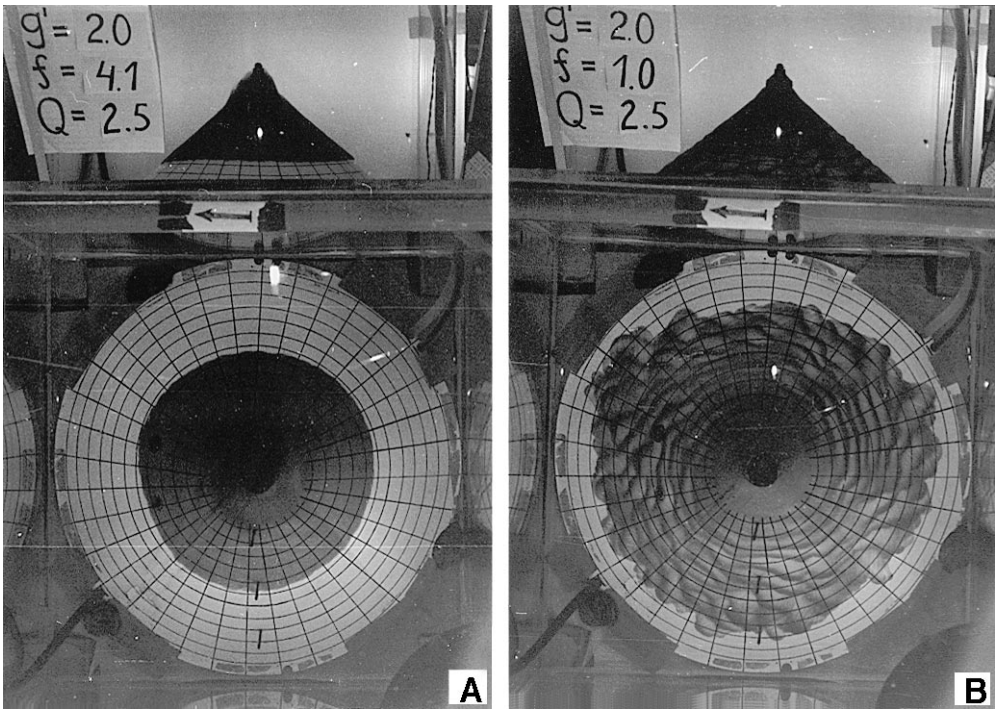

Fig. 2A, B. Top and side views of a gravity current over the cone at $t = 70$ *s* after beginning of the injection of dense fluid (coloured) at $g' = 2.0$ *cm*$/s^2$, $Q = 2.5$ *cm*$^3/S$. **A**, Stable mode: $f = 4.1$ *rad*$/s$, $Fr^* = 0.3$; **B**, oscillatory mode: $f = 1.0$ *rad*$/s$, $Fr^* = 0.8$. Here $Fr^* = u/(g'H^*)^{1/2}$ is the effective Froude number, $H^* = Q/(2\pi L u_f)$ is the effective thickness of the bottom layer

runs with very large density differences, the wave pattern became three-dimensional and irregular with interacting waves. The stability diagram is shown in Fig. 3.

Theory

Governing equations

We consider the dynamics of a two layered fluid above a circular cone rotating around a vertical axis. We introduce a curvilinear rotating orthogonal co-ordinate system so that the S-axis starts at the cone top and is directed to the foot along the cone wall, the Z-axis (local "vertical") is perpendicular to the wall of the cone, and the φ-axis is orthogonal to the S and Z axes giving a right-hand triplet.

We adopt the following non-dimensionalization scheme. Let L_0 be a typical horizontal length of the dense water plume, H_0 being its vertical length scale, and T_0 its evolution time scale. More specifically these scales will be defined differently for every basic stage of the gravity current evolution. Along-cone-wall distances are scaled by L_0, "vertical" lengths by H_0, time intervals by T_0, "horizontal" (i.e. along S and φ directions) velocities by the Nof (1983) scale $V_g = g' \sin\theta/(f\cos\theta)$, "vertical" velocities by $W = H_0 V_g/L_0$, yielding the non-dimensional variables $s, z, t, u_s, u_\varphi, u_z$ respectively. The non-dimensional pressure anomaly is introduced by the formula $p = (P - P_c)/P_0$, where $P_0 = H_0\rho_1 g' \sin\theta \times(\tan\theta + \cot\theta)$ is the hydrostatic pressure scale, $P_c = \rho_2 g\cos\theta(s\tan\theta - z)$ is the background hydrostatic pressure, ρ_1, ρ_2 – are densities of the fluid in the bottom and top layers respectively, and θ – is the bottom inclination angle.

It is assumed that the horizontal scale L_0 is much greater than the "vertical" H_0 so that the "vertical" acceleration is small and a shallow water approximation can be applied. The momentum and continuity equations for the bottom layer are written in non-dimensional variables as:

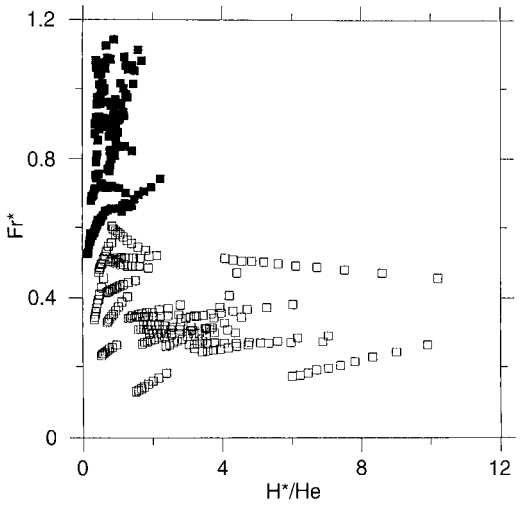

Fig. 3. Stability diagram. *Solid squares* correspond to the oscillatory mode while *open squares* correspond to the stable mode

$$\varepsilon_T \frac{\partial u_s}{\partial t} + \varepsilon\left(u_s\frac{\partial u_s}{\partial s} + \frac{u_\varphi}{s\cos\theta}\frac{\partial u_s}{\partial\varphi} - \frac{1}{s}u_\varphi^2\right) = u_\varphi + 1 + \mathsf{E}\frac{\partial^2 u_s}{\partial z^2} - \gamma\frac{\partial p}{\partial s} \tag{2}$$

$$\varepsilon_T \frac{\partial u_\varphi}{\partial t} + \varepsilon\left(u_s\frac{\partial u_\varphi}{\partial s} + \frac{u_\varphi}{s\cos\theta}\frac{\partial u_\varphi}{\partial\varphi} + \frac{u_\varphi u_s}{S}\right) = -u_s + E\frac{\partial^2 u_s}{\partial z^2} - \gamma\frac{\partial p}{s\cos\theta\partial\varphi} \tag{3}$$

$$-\varepsilon\frac{\sin\theta}{s\cos\theta}u_\varphi^2 = u_\varphi\tan\theta - \cot\theta - (\tan\theta + \cot\theta)\frac{\partial p}{\partial z} \tag{4}$$

$$\frac{\partial u_s}{\partial s} + \frac{1}{s\cos\theta}\frac{\partial u_\varphi}{\partial\varphi} + \frac{u_s}{s} + \frac{\partial u_z}{\partial z} = 0, \tag{5}$$

where the non-dimensional parameters are given by the formulas:

$$\varepsilon_T = 1/(fT_0\cos\theta), \varepsilon = V_g/(fL_0\cos\theta), E = H_E^2/H_0^2, \quad \gamma = (\tan\theta + \cot\theta)H_0/L_0. \tag{6}$$

Equations (2)–(5) take into account both "horizontal", i.e. parallel to the cone wall, (see terms $u_\varphi, -u_s$ in Eqs. (2),(3)) and "vertical", i.e. perpendicular to the cone wall, (see term $u_\varphi\tan\theta$ in Eq. 4) components of the Coriolis force. The "vertical" component is essential at steep slopes. We emphasise that at steep slopes Eq. (4) is not reduced to the hydrostatic equation even in the linear case because of the "vertical" component of the Coriolis force.

Consider the case where the thickness of the top layer is much greater than the bottom one. From momentum conservation it follows that the velocities in the top layer, induced by the motion in the bottom layer, are small. So that motion in the upper layer can be considered independently. For the purposes of this study we consider the upper fluid at rest above the interfacial Ekman layer. If necessary, the analytical technique described later can be extended to take account of the influence of motion in the top layer on the dynamics of the lower layer following the method developed for the case of a flat bottom by Shapiro (1982).

The integral form of Eq. (5) is written as

$$\varepsilon_T\frac{\partial h}{\partial t} + \varepsilon\left(\frac{1}{s}\frac{\partial}{\partial s}(sq_s) + \frac{1}{s\cos\theta}\frac{\partial q_\varphi}{\partial\varphi}\right) = 0 \tag{7}$$

where h is the nondimensional thickness of the bottom layer, q_s, q_φ are the integral specific fluxes in the bottom layer along the S and φ axes. The dimensional fluxes can be obtained by multiplication with $V_g H_0$.

The boundary conditions in the vertical are (1) no-slip conditions at the bottom, (2) continuity of the viscous stresses at the interface, and (3) vanishing of horizontal velocities in the upper layer far away from the density interface.

Next we consider axisymmetric currents ($\partial/\partial\varphi = 0$) only. The scale analysis shows that several stages or regimes can be distinguished in the dynamics of the

gravity current. The properties of these stages depend on the relative significance of the acting forces i.e. on the relationship between the non-dimensional parameters $\varepsilon, \varepsilon_T, E$, and γ.

Initial and intermediate stages

The initial stage covers the period of time comparable with a few platform rotations. We introduce the internal radius of deformation, R_0, by the formula

$$R_0 = V_g/(f\cos\theta) = (g'\sin\theta)/(f\cos\theta)^2. \tag{8}$$

Note that this definition differs from the commonly used formula and reflects the difference in the main force balance on the inclined bottom: the along-bottom component of the gravity force against the Coriolis force. Let H_0 be a typical thickness of the plume near the source, $T_0 = 1/(fcos\theta), L_0 = R_0$. In this case the parameters ε and ε_T take the value 1. We shall consider the source geometry when $L_0 \gg H_0 > H_E$, then it follows $E < 1, \gamma \ll 1$. A small pressure gradient of the order of γ is neglected, and the influence of friction (the terms of the order of E) is taken into account in the first approximation by the method of integral relations. The reason for this is that the influence of bottom and interfacial friction increases with time. Friction must then be taken into account in order to obtain matching solutions for the intermediate and main stages.

By dropping the terms proportional to γ one can obtain from Eqs. (2), (3)

$$\frac{Du_s}{Dt} - \frac{u_\varphi^2}{s} = u_\varphi + 1 + E\frac{\partial^2 u_s}{\partial z^2} \tag{9}$$

$$\frac{Du_\varphi}{Dt} - \frac{u_\varphi u_s}{s} = -u_s + E\frac{\partial^2 u_\varphi}{\partial z^2} \tag{10}$$

Similar equations for the interfacial Ekman layer in the upper layer are written as (note that the main core of the upper layer is at rest):

$$u_{\varphi 2} + E\frac{\partial^2 u_{s2}}{\partial z^2} = 0 \tag{11}$$

$$-u_{s2} + E\frac{\partial^2 u_{\varphi 2}}{\partial z^2} = 0 \tag{12}$$

The boundary condition in the upper layer far from the interface is $u_{s2} = u_{\varphi 2} = 0$ at $z \Rightarrow \infty$. Equations (9)–(12) are solved analytically using two iterations of the integral relation method. In the first iteration, the equations are integrated along the "vertical" with the assumption that the left-hand sides of Eqs. (9)–(10) are independent of the Z-coordinate. This iteration allows calculation of the approximate vertical structure of the current. In the second iteration, the Eqs. (9)–(10) are averaged over the thickness of the lower layer using the vertical structure of the current found in the first iteration. This gives the equations for the depth averaged values.

Using this technique one can obtain from Eqs. (9)–(12) the following "vertical" profile of the "horizontal" velocity which it is convenient to write down in the complex form

$$\psi = i\Phi(1 - e^{-\lambda z} - \frac{1}{2}e^{-\lambda h}(e^{\lambda z} - e^{-\lambda z})) \tag{13}$$

where

$$\begin{aligned} &\psi = u_s + iu_\varphi\,, i^2 = -1, \quad \lambda = (1+i)/\sqrt{2E}, \\ &\Phi = -2\frac{i\overline{\psi}h\lambda}{2\lambda h - 3}\,, \quad \overline{\psi} = U_s + iU_\varphi. \end{aligned} \tag{14}$$

Here U_φ, U_s are the depth averaged current velocities for the lower layer. They can be found from the following equations, obtained by depth averaging Eqs. (9), (10)

$$\begin{aligned} &\frac{DU_s}{Dt} - \frac{U_\varphi^2}{s} = (1+\alpha)U_\varphi + 1 - \alpha U_s \\ &\frac{DU_\varphi}{Dt} + \frac{U_\varphi U_s}{s} = -(1+\alpha)U_s - \alpha U_\varphi \end{aligned} \tag{15}$$

Where – $\frac{D}{Dt}$ – is the Lagrangian derivative and α is the integral friction coefficient, which is given by the formula.

$$\alpha = (3\sqrt{E})\ /\ (2h\sqrt{2}). \tag{16}$$

Analysis of Eqs. (13), (15) shows that the value of integral friction coefficient α incorporates both bottom and interfacial friction. At $E \ll 1$ the bottom friction contributes 2/3 of the total value. Note that Eqs. (15) are the ordinary (not partial) differential equations for a Lagrangian particle and are easily solved numerically. The trajectory of the Lagrangian particle is obtained then from the equations

$$\frac{Ds}{Dt} = U_s, \quad \frac{D\varphi}{Dt} = \frac{U_\varphi}{s\cos\theta}. \tag{17}$$

First we consider the initial stage of the plume evolution when the influence of friction is negligibly small, and corresponding terms in Eqs. (15) can be omitted. From the structure of Eqs. (15), the time period for the initial stage can be estimated as $t_1 \ll 1/\alpha$. Far from the top of the cone($s \gg 1$) the non-linear terms, $-(U_\varphi^2/s)$ and $(U_\varphi U_s/s)$, can be ignored, and the Eqs. (15) become linear. If the diameter of the water source, R_1, is much greater than the radius of deformation of R_0 (in non-dimensional variables $s_1 = R_1/R_0 \gg 1$) then the condition $s \gg 1$ is fulfilled along the entire trajectory, and Eqs. (15) have an analytical solution:

$$\begin{aligned} &U_s = (1 + U_{\varphi 0})\sin t + U_{s0}\cos t \\ &U_\varphi = -1 - U_{s0}\sin t + (1 + U_{\varphi 0})\cos t\,, \end{aligned} \tag{18}$$

where subscript "*0*" stands for initial ($t = 0$) conditions. By integrating the first of Eqs. (18) one gets:

$$s = s_1 + 1 + U_{s0}\sin t - (1 + U_{\varphi 0})\cos t + U_{\varphi 0}\,. \tag{19}$$

From Eq. (19) it follows that a fluid particle is trapped in a circular band around the water source. In the case of zero initial velocities the half-width of the band, Δs, is equal to 1, which in dimensional variables yields $\Delta S = R_0$. This fact reveals the physical meaning of the scale R_0 as a *radius of deformation* for a buoyancy

dominated flow over an inclined bottom : the scale R_0 determines the horizontal scale of inertial oscillations. The same scale, R_0, yields the typical value of displacement of a fluid particle along an isobath during one inertial period. It means that for a gravity current over the slope, the scale R_0 is a direct analogue to the Rossby radius for a current over a horizontal bottom. This conclusion applies also to a more general bottom topography.

At small s_1 Eqs. (15) were solved numerically using a Runge-Kutta method of the second order. The numerical results show that fluid particles are trapped in a band $s_1 < s < s_1 + 2\Delta s$ where Δs varies from $\Delta s = 1$ for $s_1 \gg 1$ to $\Delta s \approx 4$ for $s_1 \ll 1$.

At times, $t \approx 1/\alpha$ the frictional effects become important and we define this stage as an intermediate one. The trajectory of a Lagrangian particle, computed numerically from the non-linear Eqs. (15) at $\alpha = 0.05$ and $s_1 = 1.5$ is shown in Fig. 4 for a time interval $0 < t < 72$. At the intermediate stage the oscillations of the Lagrangian particle decay with time and its trajectory is transformed into a spiral. The depth averaged azimuthal $U_{\varphi c}$, and offshore, U_{Sc}, velocities tend to the following quasi stationary values:

$$U_{Sc} = \alpha/(1 + 2\alpha + 2\alpha^2)\ ,\ U_{\varphi c} = -(1 + \alpha)/(1 + 2\alpha + 2\alpha^2)\ . \tag{20}$$

It is clear from Eq. (20) that $U_{Sc} \Rightarrow 0$ both at very small and at very large values of α (i.e. at small and at large H/H_E, where H is the dimensional thickness of the bottom layer). The maximum of U_{Sc} is reached at $H = 1.5\, H_E$. From the analysis of the vertical structure of the solution [see Eqs. (13), (14), (20)] it follows that the systematic transport of a fluid down the slope occurs basically in two Ekman layers: near the bottom and near the interface.

If the source for the dense fluid is continuous, and the leakage of fluid at the outer border of the trap zone does not balance the inflow, the thickness of the trapped fluid increases. After a while the pressure gradient would outweigh the gravity force and the radius of the trap zone would be controlled by the ordinary Rossby radius $L_R = (g' \cos\theta H_0)^{1/2} / f \cos\theta$ which increases in time with H_0.

Main stage

In this section we consider the subsequent, main, stage of the evolution of the gravity current. This stage corresponds to times (dimensional) $T \gg 1(f \cos\theta)$ and distances $S \gg R_0$. In this case the parameters $\varepsilon \ll 1$, $\varepsilon_T \ll 1$, $\gamma \ll 1$ and the main momentum balance is controlled basically by buoyancy, Coriolis, and friction forces. For the main stage, it is convenient to introduce the following scales of "vertical" length, H_0, horizontal length, L_0, and time, T_0,

$$H_0 = H_E\sqrt{2}\ ,\quad L_0 = Q\ /\ (2\pi \cos\theta V_g H_E G_m),\quad T_0 = \sqrt{2}L_0\ /\ V_g\ , \tag{21}$$

where $G_m \cong 1.12$ is a numerical constant. From Eq. (21) it follows that $\varepsilon/\varepsilon_T = \sqrt{2}$, $E = 1/2$. At this stage the small terms of the order ε, ε_T, γ in the Eqs. (2), (3) can be ignored in the first approximation. By integrating the Eqs. (2), (3) over the vertical from $z = 0$ to $z = h$ we obtain the same expression (13) but in this case we have $\Phi = -1$. Then we integrate the complex fluid velocity $\psi(z)$ over the thickness of the bottom layer and take the real part of that expression. It yields the value of the downslope specific flux, q_s,

$$q_s = (3 - 4\mu(h) + \mu(2h))/4,\quad \mu(h) = e^{-h}(\cos h + \sin h) \tag{22}$$

The down slope flux q_s depends on h only and has a maximum $q_s = G_m\ /\ \sqrt{2}$ at $h = h_m = \pi$ (see Fig. 5).

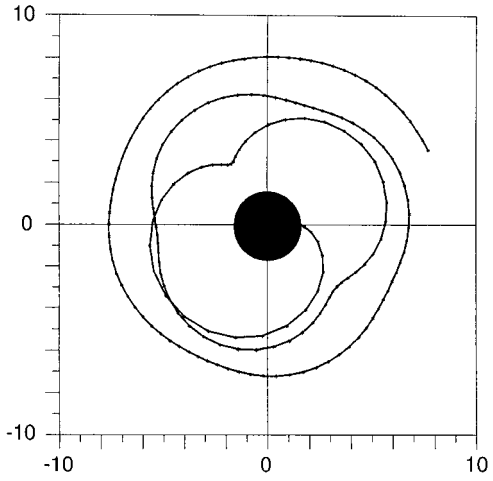

Fig. 4. Lagrangian particle trajectory at the initial and intermediate stages is shown in the polar co-ordinate system. Trajectory is computed from Eq. (8) for a value of the friction parameter $\alpha = 0.05$, a source radius $s_1 = 1.5$ for the time interval $0 < t < 72$

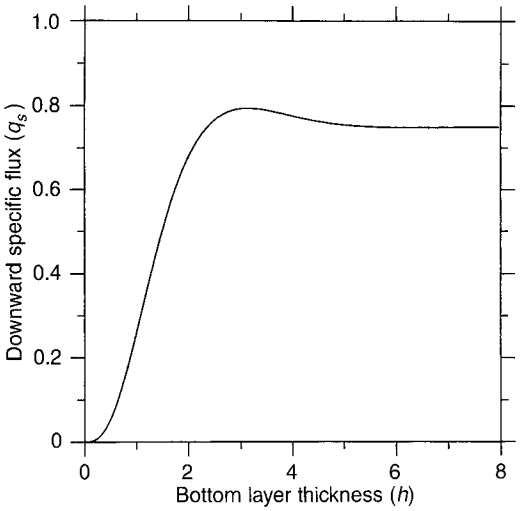

Fig. 5. Down slope specific flux, q_s, as a function of the bottom layer thickness, h, according to formula (22)

From the "vertical" velocity profile (13) we see that, similar to the intermediate stage, the downward flow is concentrated primarily in the bottom and the interfacial Ekman layers. In the inviscid core, between the two Ekman layers, the fluid velocity is directed basically along isobaths. This is why the downward flux does not increase if the thickness of the lower layer increases beyond $h = h_m$.

By substituting expression (22) into Eq. (7) we obtain a non-linear equation for $h(s,t)$. The upstream boundary condition is set at some distance, s_i, outside the trap zone: $2\pi s_i q \cos\theta = Q_i$ where the total flux, Q_i, is a constant. In the quasi stationary case, when the inflow and outflow fluxes in the trap zone are in balance, one can take $Q_i = Q$ where Q is the intensity of the source. The downstream condition is $h = 0$ at $s \Rightarrow \infty$.

At small values of $h \ll 1$ Eq. (7) has an analytical self-similar solution:

$$\begin{aligned} &h = \tfrac{C_1}{s^{1/3}} && \text{at } s < L_f, \\ &h = 0 && \text{at } s > L_f \\ &L_f = C_2 t^{3/5}\ , \end{aligned} \tag{23}$$

where $C_1 \approx 1.19$, $C_2 \approx 1.41$, and $L_f(t)$ – is the non-dimensional distance of the bottom front from the cone top as a function of time. Formulas (23) describe the down slope propagation of the dense water plume as a tongue with a steep leading edge. The thickness of the bottom layer at the edge slowly (as $t^{1/5}$) decreases with time. From Eq. (23) one can see that at $t \approx 1$, the values of L_f and h are of the order of 1. This proves that the scales introduced by Eq. (21) do have, during the main stage, the meaning of the typical thickness of the lower layer, typical length between the cone top and the bottom front, and typical evolution time respectively.

Reverting to dimensional variables we have from Eq. (23):

$$\begin{aligned} &L_f = C_3 Q^{2/5} (g')^{1/5} (\sin\theta/\cos^2\theta)^{1/5} \nu^{-1/5} t^{3/5}\ , \\ &C_3 \cong 0.69\ . \end{aligned} \tag{24}$$

In contrast to the intermediate stage, Eq. (14) does not include any dependence on the Coriolis parameter. The reason for this is that, at $h \ll 1$, the down slope current concentrates itself in the Ekman layers where the main force balance is governed by the buoyancy and friction forces. Using the technique introduced by Benney (1967), the same formulas (23), (24) can be obtained for a non-rotating fluid.

In the general case (arbitrary h) the Eqs. (7), (22) were solved numerically. A time set of successive profiles of the bottom layer thickness, $h(s)$, in the down slope direction is shown in Fig.6. The profiles were computed from Eqs. (7), (22) with boundary conditions $h = 2$ at $s = s_1 = 1.17$, (which is equivalent to $Q_1 = Q$) and $h = 0$ at $s \Rightarrow \infty$ and the initial condition $h = 0$ at $s > 1.17$. The results of computations show that the leading edge of the plume reaches the thickness of the order of 1 or less very soon even if the upstream values $h_i \gg 1$. The upstream parts of the profiles match well which supports the idea of self-similarity of the dense plume evolution. The results of computations at different boundary conditions show the similar behaviour. The computed location of the bottom front versus time is shown in Fig. 7 together with the analytical solution (23) and experimental data.

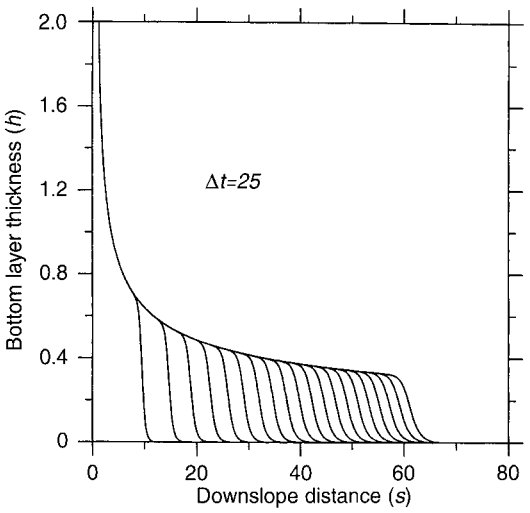

Fig. 6. A time set of successive profiles of the bottom layer thickness, $h(s)$, in the down slope direction as computed from Eqs. (7), (22) with boundary conditions $h = 2$ at $s = s_1 = 1.17$, (which is equivalent to $Q_1 = Q$) and $h = 0$ at $s \Rightarrow \infty$. Non-dimensional time interval between consecutive profiles $\Delta t = 25$

Formula (24) is not applicable to the full set of experimental data because they cover both cases $h \ll 1$, $h \approx 1$, and $h \gg 1$. Hence, the coincidence of formulas (1) and (24) should not be expected. It is however surprising that, as Fig. 7 shows, the deviation of the experimental points from the analytical curve (23) is not large.

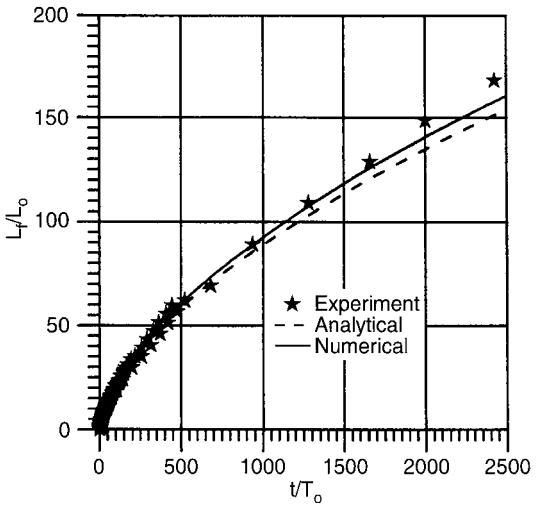

Fig. 7. Distance L_f of the gravity current front from the cone top as a function of time t in non-dimensional variables. The scales are (see Eq. 21) $L_0 = Q/(2\pi\cos\theta V_g H_E G_m)$, $T_0 = \sqrt{2}L_0/V_g$. *Stars* show experimental data, *dashed line* shows self-similar analytical solution (14), *solid line* shows the numerical solution calculated using the same boundary conditions as in Fig. 6

Instability of the main current

We consider the stability of the main current in relation to shortwave high frequency fluctuations. For the analysis of these disturbances it is necessary to take into account the pressure gradient (terms of the order of γ) and local accelerations (terms of the order of ε_T) in Eqs. (2), (3). The exact estimation of the pressure anomaly is not straightforward because of the influence of a "vertical" component of Coriolis force in the momentum balance along the Z axis (see Eq. 4). Therefore it would be inaccurate to calculate the pressure anomalies using the common "hydrostatic" approximation. The departure from the "hydrostatic" law increases with increasing bottom inclination angle.

We use the expansion of the velocity and the pressure over independent small parameters ε, ε_T, γ in Eqs. (2)–(4). The pressure gradient anomaly is calculated in the zero order approximation and includes non-hydrostatic components. The velocities and the down slope flux are calculated in the first order approximation over ε_T and γ, whereas the inertial forces of the order of ε are completely neglected. This technique is efficient at arbitrary E. In the case $E \geq 1$ (i.e. $h \leq 1$) Eq. (7) is written as:

$$\varepsilon_T \frac{\partial h}{\partial t} + \varepsilon \frac{1}{s}\frac{\partial}{\partial s}\left[s\left(\frac{h^3}{3E} + \frac{\varepsilon h^4}{144E^3}\frac{1}{s}\frac{\partial}{\partial s}(sh^3) - \frac{\gamma h^3}{3E^{3/2}}\frac{\partial h}{\partial s}\right)\right] = 0 \,. \tag{25}$$

Mathematically, Eq. (25) is a non-linear advection-diffusion equation. The first term in the square brackets represents the non-linear advection of the dense plume. The second term is produced by inertia (non-stationary terms in the momentum equations), has the opposite sign to the last term, and can be considered formally as a "non-linear negative diffusion". This term promotes the increase of fluctuations and therefore it contributes to the generation of instability. The last term originates from the velocity component produced by the pressure gradient. It can be considered as "non-linear positive diffusion" and causes the decay of fluctuations. The balance between "positive" and "negative diffusion" terms determines a threshold of instability. The order of magnitude estimation shows that the instability develops if $\varepsilon h^3 > 16\gamma E^{3/2}$. This condition can be rewritten as

$$Fr > Fr_0 = (4/3)^* 2^{1/4} (\cos\theta)^{-1} \,, \tag{26}$$

where $Fr = u_x/(g'h)^{1/2}$ is the local Froude number and $u_x = g'h^2 \sin\theta/(3\nu)$ is the depth averaged velocity in the bottom layer at $h \leq 1$.

Discussion

At the initial stage, the water parcels are involved in non-linear inertial oscillations near the cone top. The frequency of oscillation is comparable but not necessarily equal to the local Coriolis parameter $f\cos\theta$ due to the influence of the centrifugal force. The water parcels are trapped in a band whose width is several $R_0 = (g'\sin\theta)/(f\cos\theta)^2$. The scale R_0 plays a fundamental role in the dynamics of a rotating fluid over an inclined bottom, and is an analogue of the ordinary Rossby radius of deformation.

During the main stage the effective down slope spreading of dense water takes place only in the bottom and interfacial Ekman layers. This results in generation of a thin water tongue propagating down slope. Near the source, in the band of width of several R_0 the current is directed primarily along isobaths and does not contribute to the front propagation. The co-ordinate of the bottom front, L_f, computed numerically using Eqs. (7), (22) is shown in Fig. 7 as a function of time. For the sake of comparison, the scatter plot of all the original experimental data transformed into nondimensional variables using formula (21) as well as the analytical solution (23) are superimposed on the same graph. From Fig. 7 it is clear that the laboratory experiments agree well with the theoretical results for a wide range of parameter values. This agreement backs up the physics which underlies the formulas (7), (22).

In the majority of experiments we observed the stable mode of the gravity current. Sometimes it disintegrated into a set of periodic waves. Formula (26) shows that the threshold condition depends only on the Froude number and does not depend on the Ekman number. The Coriolis parameter does not influence the threshold conditions. The probable reason for this is that the oscillatory mode is generated by the instability of a thin viscous (Poiseuille) boundary layer. This fact is in a qualitative agreement with the experimental results. From Fig. 3 it follows that the oscillatory mode is observed at $Fr^* > Fr_0^* = 0.6$ while the theory gives $Fr_0 = 2.03$. This discrepancy could result from the difference in defining the theoretical (Fr, based on local velocity) and experimental (Fr^*, based on front speed) Froude numbers. Another reason might be the velocity underestimation from the measured front propagation data because they do not include the azimuthal component of the velocity. Further investigation is necessary to explain what mechanism controls the predominant wave length and non-linear stage of the disturbances.

Acknowledgements. This work was made possible partially by Russian Fund of Basic Research grants numbers 94-05-17302, 94-05-17400 and by Russian Ministry of Science and Technology projects "Hydrology of Continental Slope" and "Coastal zone. Theoretical study of physical processes". Authors are grateful to anonymous referees for their comments and K. Horsburgh of the University of Wales (UK) for his assistance in correcting the English version of the manuscript.

Topical Editor D. Webb thanks P. Baines and P. Thomas for their help in evaluating this paper.

References

Benney, D. J., Long waves on liquid films, *J. Math. Phys.*, **45**, 150–155, 1966.

Bowers, D. G., and Lennon, G. W., Observations of stratified flow over a bottom gradient in a coastal sea, *Cont. Shelf Res.* **9**, 1105–1121, 1987.

Dickson, R. R., Gmitrowicz, E. M., and Watson, A. J., Deep-water renewal in the northern North Atlantic, *Nature*, **344**, 848–850, 1990.

Kostianoy, A. G., and Shapiro, G. I., Theoretical and laboratory modelling the mesoscale anticyclonic ocean vortices, *Morsk. Gidrofiz. Z.* (in Russian) **5**, 14–21, 1985.

Latif, M. A., Ozsoy, E., Oguz, T., and Unluata, U., Observations of the Mediterranean outflow into the Black Sea, *Deep Sea Res.* **38**, s711–s723, 1991.

Mory, M., Stern, M. E., and Griffiths, R. W., Coherent baroclinic eddies on a sloping bottom. *J. Fluid Mech*. **183**, 45–62, 1987.

Nagata, Y., Kimura, R., Honji, H., Yamasaki, Y., Kawaguchi, K, and Hosoyamada T., Laboratory experiments of dense water descending on continental slope in : *Deep ocean circulation, physical and chemical aspects*. Ed. T.Teramoto, Elsevier, 333–350, 1993.

Nof, D., The translation of isolated cold eddies on a sloping bottom, *Deep-Sea Res.* **30**, 171–182, 1983.

Price, J. F., Barringer, M., Lueck, R. G., Johnson, G. C., Ambar, I., Parilla, G., Cantos, A., Kennely, M. A., and Sanford, T. B., Mediterranean outflow mixing and dynamics, *Science*, **259**, 1277–1282, 1993.

Shapiro, G. I., On the dynamics of a nonstationary atmospheric front, *Meteorol. Gidrol.* **1,** 16–23 (in Russian) 1982.

Simpson J. E., Gravity currents in the environment and the laboratory, Ellis Horwood Ltd, England, 1987.

Speer, K., Tzipperman, E., and Feliks, Y., Topography and grounding in a simple layer model, *J. Geophys. Res.* **98**, (C5) 8547–8558, 1993.

Whitehead J. A., Dense water off continents, *Nature,* **327** 656–657, 1987.

Whitehead J. A., Stern M. E., Flierl G. R., and Klinger B. A., Experimental observation of baroclinic eddies on a sloping bottom, *J. Geophys. Res.,* **95**, (C6) 9585–9610, 1990.

Zatsepin A. G., Kostianoy A. G., and Shapiro G. I. Slow spreading of a viscous fluid over a horizontal plane. *Dokl. AN SSSR,* **265**, (N1) 193–195 (in Russian), 1982.

Zatsepin A. G., On the evolution of lens-intrusion in rotating fluid, in: *Wnutritermoklinnye vikhri v okeane,* Ed. K.N.Fedorov, Moscow, IOAN, 115–119, 1986.

Zhmur V. V., Nazarenko D. V., and Prostakishin V. M., The motion of the finite volume of heavy fluid in the bottom layer of the ocean near the sloping bottom, Moscow Physical Technical Institute, Dolgoprudny, Preprint 1, 40, 1994.